

Title	Deep-Learning Generation of High-Resolution Images of Live Cells in Culture Using Tri- Frequency Acoustic Images
Author(s)	Fujiwara, Natsumi; Uno, Midori; Fukuda, Hiroki et al.
Citation	Physical Review X. 2025, 15(2), p. 021015
Version Type	VoR
URL	https://hdl.handle.net/11094/102922
rights	This article is licensed under a Creative Commons Attribution 4.0 International License.
Note	

The University of Osaka Institutional Knowledge Archive : OUKA

https://ir.library.osaka-u.ac.jp/

The University of Osaka

Deep-Learning Generation of High-Resolution Images of Live Cells in Culture Using Tri-Frequency Acoustic Images

Natsumi Fujiwara,* Midori Uno,* Hiroki Fukuda, Akira Nagakubo, Shao Ying Tan, Masahiro Kino-oka, and Hirotsugu Ogio[†]

Graduate School of Engineering, Osaka University, Yamadaoka 2-1, Suita, Osaka 565-0871, Japan

(Received 7 June 2024; revised 10 December 2024; accepted 13 March 2025; published 15 April 2025)

Ultrasound microscopy is the only technique that has the ability to monitor live-cell morphology over a long period of time without causing any damage to the cells, but its longer wavelength prevents one from obtaining high-resolution cell images. Here, we propose a deep-learning (DL) method for generating high-resolution acoustic images. By preparing datasets consisting of many pairs of acoustic and opticalmicroscope images for the same cells and training them, a high-resolution image comparable to optical microscopy is generated from an acoustic image. Importantly, the most accurate images are generated when three-layer (RGB) images containing not only high-frequency (approximately 180 MHz) images but also lower-frequency (approximately 100 MHz) images are used as the input images, which is attributed to enhanced acoustic absorption in the nucleus because the nucleus resonates in this low-frequency band. The DL scheme with the tri-frequency image input is applied to human mesenchymal stem cells and human induced pluripotent stem cells, and the high image-generation capability is demonstrated. As a result, highresolution acoustic microscopy images are obtained for the same cells for over 24 h, without the typical cell damage encountered using optical imaging.

DOI: 10.1103/PhysRevX.15.021015 Subject Areas: Acoustics, Biological Physics, Computational Physics

I. INTRODUCTION

Cell imaging is crucial for assessing morphology, microstructure, and cellular status, and various techniques have been accordingly used, including optical microscopy [1], atomic-force microscopy [2], and electron microscopy [3]. Especially, live-cell imaging, which dynamically observes changes in the morphology and internal structure of live cells, has been one of the challenging tasks in understanding the biological complexity of cells. For this purpose, optical-microscopic techniques such as wide-field microscopy [4], light-sheet microscopy [5], and superresolution microscopy [6] have been adopted, but they require long-time and high-intensity light exposure to obtain high-resolution images with a sufficient signal-tonoise ratio [1,7–9]. However, light irradiation is known to damage cells, because intercellular organic molecules such as flavins absorb visible light [10] and react with oxygen. This process produces reactive oxygen species, including

Published by the American Physical Society under the terms of the Creative Commons Attribution 4.0 International license. Further distribution of this work must maintain attribution to the author(s) and the published article's title, journal citation, and DOI.

radicals and hydrogen peroxide, which oxide proteins and DNA, resulting in degradation of cell functions [7,11–15]. Much research appeared to reduce the photoinvasiveness to cells, including optimization of light irradiation [12,16,17], use of highly sensitive CCD camera for detecting weak fluorescent signals [18], and addition of cell-protective reagents [19].

In recent years, deep-learning (DL) achieves dramatic improvements in live-cell imaging [20,21]. Noise removal [22,23], restoration [24–26], and label-free imaging [27,28] using DL realized high-resolution images with short exposure times. These efforts have reduced some of the damage to cells caused by light irradiation, but, as long as light irradiation is involved, the fundamental issue remains unresolved. As a result, continuous (or high-frame-rate) and high-resolution observation of the same cell for approximately 24 h or longer has remained difficult.

On the other hand, scanning acoustic microscopy (SAM) is essentially capable of solving the problems mentioned above, because it creates images using acoustic properties without light irradiation, labeling, and mechanical contact to the cell. However, its spatial resolution is considerably poorer than that of optical microscopy because of longer ultrasound wavelength. In addition, because it has been difficult to incorporate the specialized equipment of SAM within a stable culture environment, SAM has been limited to observation of cells outside the culture environment.

These authors contributed equally to this work. †Contact author: ogi@prec.eng.osaka-u.ac.jp

Therefore, SAM has been used for a short-time measurement of mechanical properties and three-dimensional shapes of cells [29–31] and not for a long-time monitoring of changes in the morphology and microstructure of cells in culture.

To overcome these problems and demonstrate the effectiveness of SAM for live-cell imaging, we propose a DL method to generate a high-resolution image from an acoustic image. Various studies have been proposed to improve the resolution of the acoustic image with DL [32–34], but no research has achieved the creation of cell images with resolution comparable to those of optical microscopy. We here propose using a three-layer (RGB) acoustic image as an input, which is composed of the spectroscopic acoustic images at three different frequencies. After the SAM measurement, we obtain the corresponding optical image for the same cell as the answer image. We, thus, prepare many input-output pairs (dataset) and train them with our original convolutional neural network (CNN). Importantly, we find that an RGB image composed not only of images of higher frequencies (approximately 180 MHz), but also of lower frequencies (approximately 100 MHz) can most accurately produce the cell structure including the nucleus, because the nucleus is acoustically stained near 100 MHz due to the nucleus resonance [35]. By investigating the combinations of the frequency images to be used in the RGB image, we identify ideal frequency combinations to generate high-resolution images, focusing on the nucleus and cell shape. We adopt our DL method to the long-time monitoring of human mesenchymal stem cells (MSCs) and human induced pluripotent stem cells (iPSCs) without interrupting cell culturing.

II. EXPERIMENTAL SECTION

A. Scanning-acoustic-microscopy system for live-cell imaging

The details of our SAM system are given in the previous paper [35], and we briefly present it. The cell-culture environment is realized in an acrylic container, where the gas is filled with air containing 5% CO₂, and the temperature and humidity are maintained at 37 °C and 100%, respectively. A cell-culture dish is placed in the container to culture cells for longer than 24 h. There is a hole on the top surface of the container, through which the acoustic lens of the SAM comes into contact with the culture medium in the culture dish, and the focused ultrasound is transmitted through the culture medium to the cell. The gap between the acoustic lens and the hole is sealed by a flexible rubber film to prevent contamination from the outside environment.

The longitudinal-wave pulse with a center frequency of 180 MHz is launched from the acoustic lens, focused and propagated inside the cell, reflected on the culture surface, and then detected by the same acoustic lens. By performing the fast-Fourier-transformation procedure for the echo from

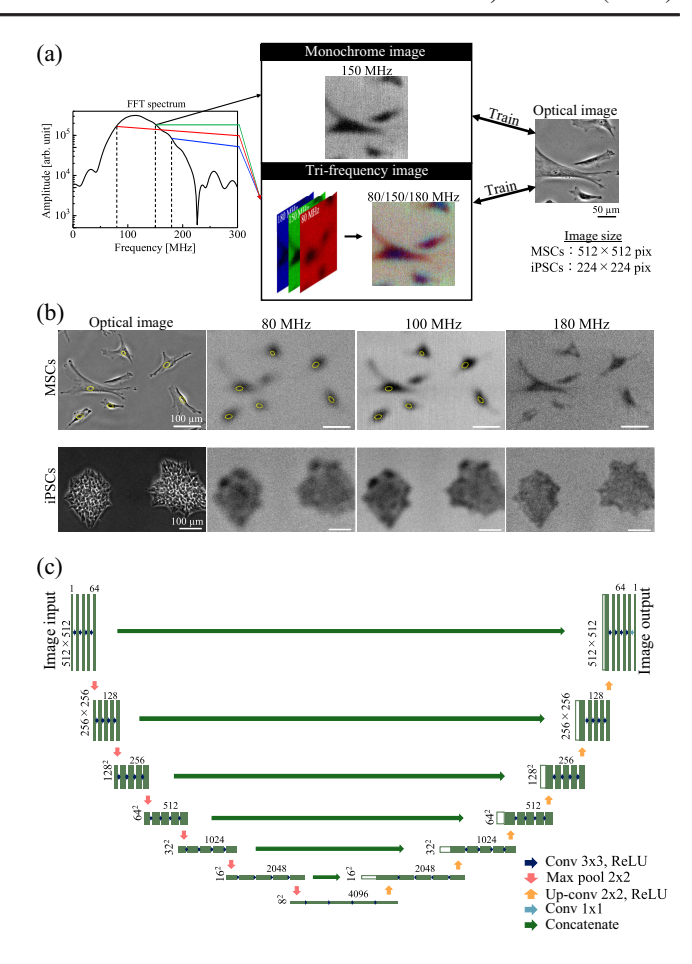


FIG. 1. (a) Construction of the spectroscopic acoustic images for preparing the datasets. (b) Representative optical and the spectroscopic acoustic images of MSCs and iPSCs. Yellow broken lines in MSCs images indicate nuclei. (c) The CNN scheme developed for generating MSCs images.

the culture surface, we obtain the amplitude spectrum as shown in the left figure in Fig. 1(a). (The center frequency of the detected echoes decrease from 180 to 100 MHz. This is because high-frequency components of the ultrasound are attenuated in the culture medium.) Acquiring the spectra by scanning the cell with the acoustic probe, we construct eight-bit images of specific frequencies (spectroscopic images) as shown in the middle figure in Fig. 1(a).

B. Cell preparation

MSCs derived from umbilical cord are used in this study, which were approved by the ethical committee of Hyogo Medical University (202308-020). The cell-culture method and the reagents used are the same as in the previous study [35].

In preparing the images for the dataset, the cells are fixed by applying a 4% paraformaldehyde solution (Fujifilm Wako Pure Chemical Corp., Japan) when the confluence reaches 70%, incubated for 10 min at room temperature, and rinsed with phosphate buffered saline solution. The optical-microscopy observation is then performed, followed by the acoustic spectroscopic measurement for obtaining optical and acoustical images for the same cells.

iPSCs (1383D2 cell line) are from the Center for iPS Cell Research and Application at Kyoto University [36]. A 35-mm-diameter culture dish (ibidi GmbH, Germany) coated with laminin-511 E8 fragments (Nippi, Inc., Japan) is used, in which the single cells are seeded as 2.5×10^3 cells/cm² with 10 μM Rho-associated protein kinase inhibitor (Fujifilm Wako Pure Chemical Corp., Japan). A 1% antibiotic-antimycotic agent (ThermoFisher Scientific, Japan) is added after 72 h from the cell seeding. In preparing the dataset images, the cells are fixed by the same method described above, followed by the optical and then SAM observations.

C. Optical-microscopic measurement

After fixing the cells, the optical-microscopy images are obtained by using a phase contrast microscope with a $10 \times$ objective lens.

Figure 1(b) shows examples of the acoustic spectroscopic images for MSCs and iPSCs at three different frequencies and their corresponding optical-microscopy images.

III. DEEP-LEARNING SCHEME

We prepare 109 824 sets of acoustic spectroscopic images and corresponding optical-microscopic images for MSCs and 55 396 sets for iPSCs. Image sizes are 512 pixels square for MSCs and 224 pixels square for iPSCs. As the input acoustic image, we use the monochrome image at a specific frequency and the RGB image composed of acoustic images of three frequencies and examine the quality of the generated images by changing the frequency in the monochrome image and the combination of the three frequencies in the RGB image. These datasets are trained using the CNN shown in Fig. 1(c) by Deep Learning Toolbox of MATLAB (version R2024a). It is based on U-Net [37], but we increase the number of the convolution-ReLU (rectified linear unit) sequence from two to four in both the contracting and expansive pathways. In addition, we use a deeper network. These modification considerably improves the quality of the generated images.

This network is trained using the adaptive-moment-estimation (Adam) optimizer. More than 95% of the dataset is used for training and the remainder for validation. Since a variety of input acoustic images are examined, the corresponding dataset for each is prepared and independently trained. The normalized root-mean-squared error for each pixel (0–1) after training is about 0.05 and 0.15 for MSCs and iPSCs, respectively. The training procedure takes nearly three days in the case of our desktop PC [CPU, Intel Core i9-14900K (24 cores, 3.2 GHz, 2.4 GHz); RAM,

Crucial DDR5 48 GB \times 2 (3200 MHz); GPU, Nvidia Geforce RTX 4090 (RAM 24 GB)].

IV. RESULTS AND DISCUSSION

A. Generation of MSC image

Figure 2 compares output (generated) images from various spectroscopic acoustic images (inputs) that are not included in the dataset for training and validation. (Other examples are shown in Supplemental Fig. S1 [38].)

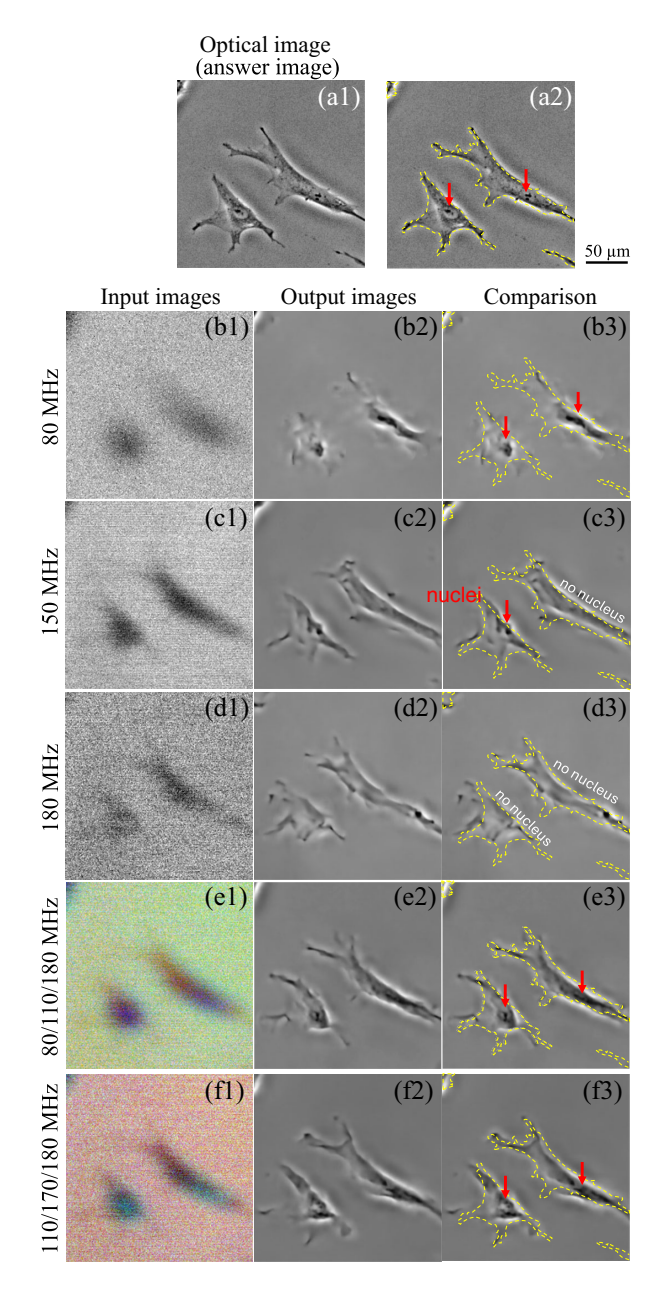


FIG. 2. The optical (answer) image, spectroscopic acoustic images as inputs (left line), output (generated) images (middle line), and comparison images from the answer image (right line) of MSCs. The yellow broken line shows the cell shape of the optical image (a2), and red arrows indicate nuclei in each image.

The resolution of the generated images is greatly improved compared to that of the original acoustic images, and it is comparable to that of the optical image, demonstrating that the DL scheme developed in this study is highly effective. The high-frequency (180 MHz) monochrome image is able to reproduce the cell's contour shape [Fig. 2(d2)] as expected owing to the shorter wavelength. However, it often fails to reproduce the nucleus as shown in Fig. 2(d3) and Supplemental Fig. S1(a) [38]. On the other hand, lower-frequency (< ~100 MHz) acoustic images have superior ability to reproduce the cell nucleus [Figs. 2(b2) and 2(b3) and Supplemental Fig. S1 [38]].

We attribute this to the mechanical resonance of the nucleus [35]. The optical-microscopy observation indicates that the diameter of the nucleus of MSC is about 20 µm [Supplemental Fig. S2(a) [38]], which yields the resonance frequency of the breathing mode to be 77 MHz assuming the longitudinal-wave and shear-wave velocities of the nucleus to be 1550 and 80 m/s, respectively [39]. Although the nucleus diameter evaluated from the 2D observation is expected to be larger than the effective 3D diameter for the cells on the culture dish, suggesting a higher resonant frequency, the resonant vibration of the nucleus should be accompanied by a greater dissipation of acoustic energy in the liquid, which lowers the resonance frequency and greatly increases the peak width. Thus, small frequency deviations from the resonance can be considered equivalent to the resonant state due to the broadness of the peak width. Actually, the absorption of the acoustic energy by nucleus at 80 MHz can be clearly confirmed in Fig. 2(b1) and Supplemental Fig. S1 [38]. Furthermore, this suggests that the nucleus fails to absorb the acoustic energy at this low-frequency band when the nucleus membrane is disassembled. Figure 3 supports this view: It shows two cells that happen to be observed during cell division. They are considered to be in the state when the nuclear membrane is temporarily disassembled during the early to middle stage of cell division. At higher frequencies, the presence of materials constituting the nucleus clearly appears. However, at 80 MHz, there is almost no acoustic absorption, because the nucleus cannot resonate any more without its membrane, and its wavelength is too long to sense them.

These findings given by the monochrome-image inputs inspire the strategy of involving higher and lower frequencies in the input acoustic image. We, therefore, construct

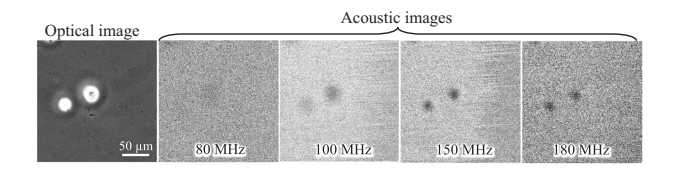


FIG. 3. Optical and spectroscopic acoustic images for MSCs in the early to middle state of cell division.

the three-layer (RGB) input images consisting of various frequency images and trained them [Fig. 1(a)]. As a result, it is found that the RGB image composed of 80, 110, and 180 MHz frequency images can accurately generate both the contour shape and nucleus as shown in Fig. 2 and Supplemental Fig. S1 [38] for a variety of cell morphologies. Figure 4 shows intersection over union (IoU) values for cell shape and nucleus of MSCs between the generated and optical (answer) images. IoU is a metric to evaluate the accuracy of the predicted image, and it is defined as the ratio of the overlapping area between the area of the target in the generated image and that in the ground-truth image (i.e., optical image) to the area of their union obtained by summing their areas and then subtracting the overlapping area. It takes from 0 to 1, and a higher IoU value indicates a better prediction.

As shown in Fig. 4(a), the IoU for the cell shape is about 0.6, except for the 80-MHz monochrome-image input, which deteriorates it to approximately 0.4 due to the longer wavelength. Comparison of the IoU values for the same cells reveals that the IoU values of the RGB acoustic inputs are significantly higher than those of the monochrome frequency inputs, especially for the RGB input of 80, 110, and 180 MHz frequency image. Furthermore, this trend becomes more remarkable in the IoU for the nucleus generation as shown in Fig. 4(b). Thus, using this RGB acoustic image, it is possible to construct high-resolution live-cell images without damaging the cells. Supplemental Movie S1 [38] demonstrates this. The SAM is used to obtain the acoustic image for 24 h with the system described in Sec. II A. The left movie in Movie S1 [38] consists of the standard acoustic images at the highest echo

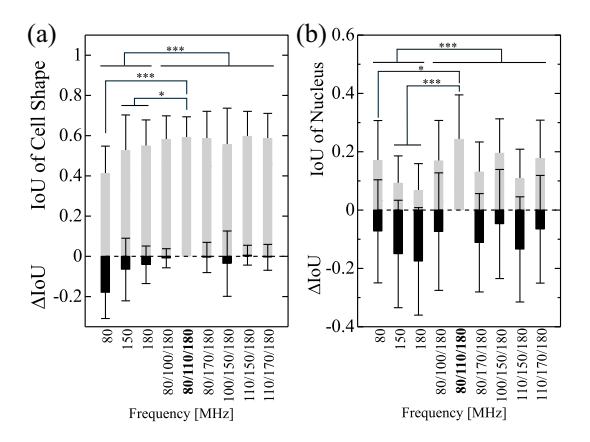


FIG. 4. IoU values for (a) cell shape and (b) nucleus region for MSCs for various acoustic image inputs (gray bars), which are calculated from the pairs of the generated and the ground-truth (optical) images from 30 randomly selected pairs. The error bars indicate the standard deviation. The black bars show the difference in the IoU values with respect to that for the $80/110/180~\mathrm{MHz}$ input for the same images ($\Delta\mathrm{IoU} = \mathrm{IoU} - \mathrm{IoU}_{80/110/180~\mathrm{MHz}}$). The p values for the paired data are calculated with the one-side t test. (*, p < 0.05; ***, p < 0.001.)

amplitude, and the right movie is generated by the DL method using the 80/110/180 MHz RGB input. The latter shows more clearly the filopodia at the edge of the cell that extends as the cells migrate and the movement of the nucleus within the cell, indicating a significant improvement in resolution compared to the original movie.

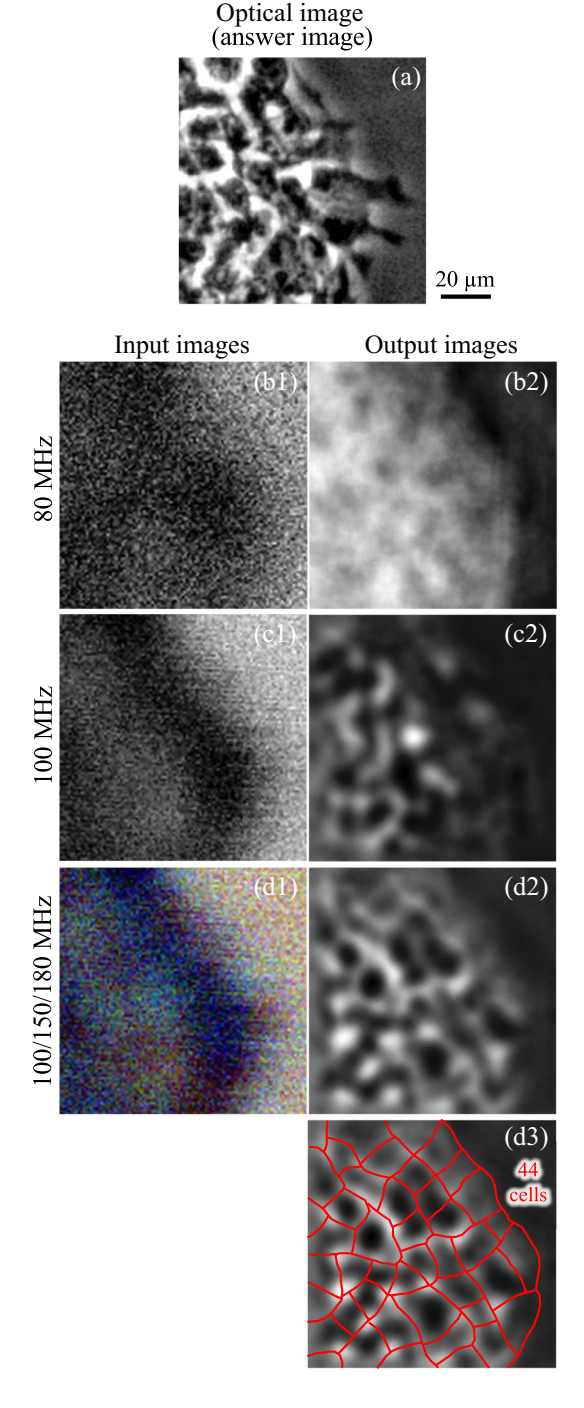


FIG. 5. The optical (answer) image (top), spectroscopic acoustic images as inputs (left line), and output (generated) images (right line) for iPSC colony. Red lines in (d3) indicate individual cells in the generated image.

B. Generation of iPSC colony image

It is more challenging to generate high-quality images for iPSCs in culture, because they gather together to form a colony, within which proliferation and migration of cells proceed [40–43], so that the cells are often overcrowded and not easily distinguished even by an optical microscopy. For iPSCs, it is more important to evaluate the properties of a colony than to reproduce the position of each individual cell in the colony, and accurate evaluation of the total number of cells and cell density in the colony is required. Therefore, we focus on predicting the number of cells in the colony and the colony size.

Figure 5 compares the optical image and generated images with various acoustic inputs for a part of iPSC colony. Unlike for the MSCs case, little contrast of cells within colony is obtained at the 80 MHz ultrasound as shown in Fig. 5(b2). This may be attributed to the fact that nuclei of iPSCs are smaller than those of MSCs as seen in Supplemental Fig. S2 [38]. Using the nucleus diameter of iPSCs of about 14 µm obtained from Supplemental Fig. S2(b) [38], the resonance frequency of the nucleus is expected to exceed 100 MHz. Therefore, we use spectroscopic acoustic images of frequencies higher than 100 MHz for constructing the RGB inputs. After examining various frequency combinations, we find that the RGB acoustic images composed at frequencies of 100, 150, and 180 MHz yield favorable results as shown in Fig. 5(d) and Supplemental Fig. S3 [38], allowing estimation of the number of cells in the colony as shown in Fig. 5(d3).

Supplemental Movie S2 [38] compares the standard acoustic images and those generated by the DL method using the RGB input for iPSC colonies. The generated movie again much more clearly shows changes of cell behavior inside the colonies, and we count the number of regions within each colony that appear to be cells. Figure 6 shows evolutions of the number of cells, colony area, and cell-number density for three colonies evaluated from the generated images in Supplemental Movie S2 [38].

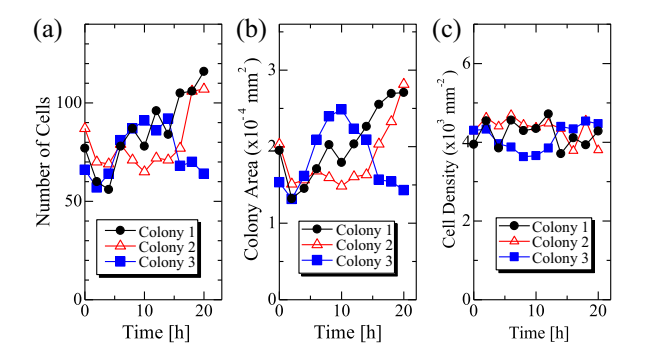


FIG. 6. Changes in (a) cell number in each colony, (b) colony area, and (c) cell-number density evaluated by the generated images (right movie in Supplemental Movie S2 [38]). Colonies 1, 2, and 3 denote top-right, left, and bottom-right colonies, respectively, in Movie S2.

Because both the number of cells and the area of colony increase with time, the number density of cells remains nearly constant at $4-5 \times 10^3$ cells/mm². This trend is consistent with previous reports [41]. Furthermore, the cell-density value obtained here is in good agreement with those reported. For example, Wakao *et al.* [44] showed that the cell density in iPSC colonies becomes approximately 6×10^3 cells/mm². Suga *et al.* [41] found the value to be $2.3-6.5 \times 10^3$ cells/mm², depending on the cell line, culture conditions, colony morphology, and so on. This concordance of qualitative and quantitative evaluations strongly supports the utility of the DL method constructed in this paper.

V. CONCLUSIONS

We proposed a deep-learning methodology for generating high-resolution images from images obtained by scanning acoustic microscopy. By preparing the dataset consisting of many spectroscopic acoustic images and corresponding optical-microscopy images and training it, the resolution of the generated images was comparable with that of the optical microscopy. The key was to use a three-layer RGB input and to involve not only high-frequency acoustic image, but also (or more importantly) low-frequency acoustic images in the RGB input, because the cell nucleus can absorb the acoustic energy of lower frequencies through its mechanical resonance. This DL method was successfully applied to MSCs and iPSCs. The cell density in the iPSC colony evaluated in this method well agrees with those reported.

Because SAM is virtually noninvasive and does not damage cells, it allows live-cell observation of the same cell for a very long time with a high frame rate. The only drawback of SAM is its low resolution, but the trifrequency RGB method proposed in this paper greatly improved this drawback. Further improvement of the network structure and training of the dataset with stained high-resolution images will make it possible to achieve even higher resolution, which will be our future work.

ACKNOWLEDGMENTS

We thank professor Nagatoshi Fujiwara of Tezukayama University for his technical assistance in cell observation. This work was supported by JSPS KAKENHI Grant No. JP24H00045.

N. F. developed the SAM system, performed the spectroscopic SAM experiments, prepared the dataset, analyzed data, and wrote the paper. M. U. developed the CNN structure, prepared the dataset, and analyzed data. H. F. contributed to development of the CNN structure. A. N. contributed to discussions and data analysis. S. T. and M. K. prepared the MSCs and iPSCs and contributed to discussions. H. O. promoted this study and wrote the paper.

- [1] D. J. Stephens and V. J. Allan, *Light microscopy techniques* for live cell imaging, Science **300**, 82 (2003).
- [2] Y. F. Dufrêne, T. Ando, R. Garcia, D. Alsteens, D. Martinez-Martin, A. Engel, C. Gerber, and D. J. Müller, *Imaging modes of atomic force microscopy for application in molecular and cell biology*, Nat. Nanotechnol. **12**, 295 (2017).
- [3] J. R. McIntosh, *Electron microscopy of cells: A new beginning for a new century*, J. Cell Biol. **153**, F25 (2001).
- [4] J. R. Swedlow and M. Platani, Live cell imaging using widefield microscopy and deconvolution, Cell Struct. Funct. 27, 335 (2002).
- [5] N. R. Subedi, S. Stolyar, S. J. Tuson, C. J. Marx, and A. E. Vasdekis, *Scattered-light-sheet microscopy with sub-cellular resolving power*, J. Biophoton. **16**, e202300068 (2023).
- [6] A. Godin, B. Lounis, and L. Cognet, Super-resolution microscopy approaches for live cell imaging, Biophys. J. 107, 1777 (2014).
- [7] E. C. Jensen, Overview of live-cell imaging: Requirements and methods used, Anat. Rec. 296, 1 (2013).
- [8] R. Cole, Live-cell imaging, Cell Adhes. Migr. 8, 452 (2014).
- [9] M. M. Frigault, J. Lacoste, J. L. Swift, and C. M. Brown, Live-cell microscopy—Tips and tools, J. Cell Sci. 122, 753 (2009).
- [10] J. Rösner, A. Liotta, E. Angamo, C. Spies, U. Heinemann, and R. Kovács, *Minimizing photodecomposition of flavin* adenine dinucleotide fluorescence by the use of pulsed LEDs, J. Microsc. 264, 215 (2016).
- [11] R. J. Wang, Effect of room fluorescent light on the deterioration of tissue culture medium, In vitro 12, 19 (1976).
- [12] J. Icha, M. Weber, J. C. Waters, and C. Norden, *Phototoxicity in live fluorescence microscopy, and how to avoid it*, BioEssays **39**, 1700003 (2017).
- [13] J.-Y. Tinevez, J. Dragavon, L. Baba-Aissa, P. Roux, E. Perret, A. Canivet, V. Galy, and S. Shorte, in *Imaging and Spectroscopic Analysis of Living Cells*, Methods in Enzymology Vol. 506, edited by P. M. Conn (Academic, New York, 2012), Chap. 15, pp. 291–309.
- [14] V. Magidson and A. Khodjakov, *Circumventing photo-damage in live-cell microscopy*, Methods Cell Biol. **114**, 545 (2013).
- [15] S. Wäldchen, J. Lehmann, T. Klein, S. van de Linde, and M. Sauer, *Light-induced cell damage in live-cell super-resolution microscopy*, Sci. Rep. **5**, 15348 (2015).
- [16] V. Magidson and A. Khodjakov, in *Digital Microscopy*, Methods in Cell Biology Vol. 114, edited by G. Sluder and D. E. Wolf (Academic, New York, 2013), Chap. 23, pp. 545–560.
- [17] W. C. Lemon and K. McDole, *Live-cell imaging in the era of too many microscopes*, Curr. Opin. Cell Biol. **66**, 34 (2020).
- [18] H. T. Beier and B. L. Ibey, Experimental comparison of the high-speed imaging performance of an EM-CCD and SCMOS camera in a dynamic live-cell imaging test case, PLoS One 9, e84614 (2014).
- [19] J. H. Stockley, K. Evans, M. Matthey, K. Volbracht, S. Agathou, J. Mukanowa, J. Burrone, and R. T. Káradóttir, Surpassing light-induced cell damage in vitro with novel cell culture media, Sci. Rep. 7, 849 (2017).
- [20] C. Belthangady and L. A. Royer, *Applications, promises, and pitfalls of deep learning for fluorescence image reconstruction*, Nat. Methods **16**, 1215 (2019).

- [21] J. W. Pylvänäinen, E. G. de Mariscal, R. Henriques, and G. Jacquemet, *Live-cell imaging in the deep learning era*, Curr. Opin. Cell Biol. 85, 102271 (2023).
- [22] H. Wang, Y. Rivenson, Y. Jin, Z. Wei, R. Gao, H. Günaydın, L. A. Bentolila, C. Kural, and A. Ozcan, *Deep learning enables cross-modality super-resolution in fluorescence microscopy*, Nat. Methods 16, 103 (2019).
- [23] R. F. Laine, G. Jacquemet, and A. Krull, *Imaging in focus: An introduction to denoising bioimages in the era of deep learning*, Int. J. Biochem. Cell Biol. **140**, 106077 (2021).
- [24] M. Weigert et al., Content-aware image restoration: Pushing the limits of fluorescence microscopy, Nat. Methods 15, 1090 (2018).
- [25] B. Zhu, J. Z. Liu, S. F. Cauley, B. R. Rosen, and M. S. Rosen, *Image reconstruction by domain-transform mani*fold learning, Nature (London) 555, 487 (2018).
- [26] W. Ouyang, A. Aristov, M. Lelek, X. Hao, and C. Zimmer, Deep learning massively accelerates super-resolution localization microscopy, Nat. Biotechnol. 36, 460 (2018).
- [27] C. Ounkomol, S. Seshamani, M. M. Maleckar, F. Collman, and G. R. Johnson, Label-free prediction of threedimensional fluorescence images from transmitted-light microscopy, Nat. Methods 15, 917 (2018).
- [28] E. M. Christiansen, S. J. Yang, D. M. Ando, A. Javaherian, G. Skibinski, S. Lipnick, E. Mount, A. O'Neil, K. Shah, A. K. Lee, P. Goyal, W. Fedus, R. Poplin, A. Esteva, M. Berndl, L. L. Rubin, P. Nelson, and S. Finkbeiner, *In silico labeling: Predicting fluorescent labels in unlabeled images*, Cell 173, 792 (2018).
- [29] A. Kinoshita, S. Senda, K. Mizushige, H. Masugata, S. Sakamoto, H. Kiyomoto, and H. Matsuo, Evaluation of acoustic properties of the live human smooth-muscle cell using scanning acoustic microscopy, Ultrasound Med. Biol. 24, 1397 (1998).
- [30] E. M. Strohm and M. C. Kolios, Measuring the mechanical properties of cells using acoustic microscopy, in Proceedings of the 2009 Annual International Conference of the IEEE Engineering in Medicine and Biology Society (IEEE, New York, 2009), p. 6042, 10.1109/IEMBS.2009.5334535.
- [31] P. Anastasiadis and P. V. Zinin, *High-frequency time-resolved scanning acoustic microscopy for biomedical applications*, Open Neuroimaging J. **12**, 69 (2018).
- [32] R. J. G. van Sloun, R. Cohen, and Y. C. Eldar, *Deep learning in ultrasound imaging*, Proc. IEEE 108, 11 (2020).
- [33] Ákos Makra, W. Bost, I. Kalló, A. Horváth, M. Fournelle, and M. Gyöngy, *Enhancement of acoustic microscopy lateral resolution: A comparison between deep learning and two deconvolution methods*, IEEE Trans. Ultrason. Ferroelectr. Freq. Control **67**, 136 (2020).
- [34] P. Banerjee, S. Akarte, P. Kumar, M. Shamsuzzaman, A. Butola, K. Agarwal, D. Prasad, F. Melandso, and A. Habib, *High-resolution imaging in acoustic microscopy using*

- deep learning, Machine Learning: Sci. Technol. 5, 015007 (2024).
- [35] N. Fujiwara, S. Y. Tan, T. Matsumoto, A. Nagakubo, M. Kino-oka, and H. Ogi, Development of a focused-ultrasound spectroscopic-imaging system combined with optical imaging for applying mechanical stimulation on living cells and the possibility of selective stimulation for the nucleus, Jpn. J. Appl. Phys. 63, 03SP65 (2024).
- [36] M. Nakagawa, Y. Taniguchi, S. Senda, N. Takizawa, T. Ichisaka, K. Asano, A. Morizane, D. Doi, J. Takahashi, M. Nishizawa, Y. Yoshida, T. Toyoda, K. Osafune, K. Sekiguchi, and S. Yamanaka, A novel efficient feeder-free culture system for the derivation of human induced pluripotent stem cells, Sci. Rep. 4, 3594 (2014).
- [37] O. Ronneberger, P. Fischer, and T. Brox, *U-net: Convolutional networks for biomedical image segmentation*, in *Medical Image Computing and Computer-Assisted Intervention—MICCAI 2015*, edited by N. Navab, J. Hornegger, W. M. Wells, and A. F. Frangi (Springer International Publishing, Cham, 2015), pp. 234–241.
- [38] See Supplemental Material at http://link.aps.org/supplemental/10.1103/PhysRevX.15.021015 for figures that show generated images for various MSCs (S1) and iPSC colonies (S3) and nuclei of MSCs and iPSCs (S2). Movies S1 and S2 show standard time-lapse images obtained by SAM and those by the DL method for MSCs and iPSCs, respectively.
- [39] V. Galstyan, O. S. Pak, and H. A. Stone, A note on the breathing mode of an elastic sphere in Newtonian and complex fluids, Phys. Fluids 27, 032001 (2015).
- [40] R. Kato, M. Matsumoto, H. Sasaki, R. Joto, M. Okada, Y. Ikeda, K. Kanie, M. Suga, M. Kinehara, K. Yanagihara, Y. Liu, K. Uchio-Yamada, T. Fukuda, H. Kii, T. Uozumi, H. Honda, Y. Kiyota, and M. K. Furue, *Parametric* analysis of colony morphology of non-labelled live human pluripotent stem cells for cell quality control, Sci. Rep. 6, 34009 (2016).
- [41] M. Suga, H. Kii, K. Niikura, Y. Kiyota, and M. K. Furue, Development of a monitoring method for nonlabeled human pluripotent stem cell growth by time-lapse image analysis, Stem Cells Transl. Med. 4, 720 (2015).
- [42] S. K. Schnyder, J. J. Molina, and R. Yamamoto, Control of cell colony growth by contact inhibition, Sci. Rep. 10, 6713 (2020).
- [43] T. N. T. Nguyen, K. Sasaki, and M. Kino-oka, *Elucidation* of human induced pluripotent stem cell behaviors in colonies based on a kinetic model, J. Biosci. Bioeng. **127**, 625 (2019).
- [44] S. Wakao, M. Kitada, Y. Kuroda, F. Ogura, T. Murakami, A. Niwa, and M. Dezawa, *Morphologic and gene expression criteria for identifying human induced pluripotent stem cells*, PLoS One **7**, e48677 (2012).